Engineering Structures 114 (2016) 122–134

Contents lists available at ScienceDirect

Engineering Structures

journal homepage: www.elsevier.com/locate/engstruct

Design optimization of a MASH TL-3 concrete barrier using RBF-based metamodels and nonlinear finite element simulations

Hanfeng Yin [a,b], Hongbing Fang [b,*], Qian Wang [c], Guilin Wen [a]

[a] State Key Laboratory of Advanced Design and Manufacturing for Vehicle Body, Hunan University, Changsha, Hunan 410082, PR China
[b] Department of Mechanical Engineering and Engineering Science, The University of North Carolina at Charlotte, Charlotte, NC 28223, USA
[c] Department of Civil and Environment Engineering, Manhattan College, Riverdale, NY 10471, USA

ARTICLE INFO

Article history:
Received 14 October 2015
Revised 1 February 2016
Accepted 5 February 2016

Keywords:
Optimization
Concrete barrier
Crash simulation
Finite element (FE)
Radial basis function (RBF)
Genetic algorithm (GA)

ABSTRACT

Concrete barriers are one of the most widely used safety features for preventing errant vehicles from entering opposing travel lanes on highways. As a safety device, a concrete barrier is also required to safely redirect a striking vehicle such that it is not bounced into travel lanes and collide with other vehicles. Given its rigidity compared to most vehicular structures, the performance of a concrete barrier is mainly influenced by its shape or the cross-sectional geometry. Over the years, concrete barriers have been continuously improved using roadway crash data and crash tests. Although the current in-service concrete barriers satisfy the requirements of safety standards, the empirical approach is not cost-effective for designing new barrier systems. In this study, a simulation-based optimization approach was adopted to obtain the optimum design of a concrete barrier by combining nonlinear finite element (FE) simulations, metamodeling with radial basis functions (RBFs), and a genetic algorithm (GA). The performance of the concrete barrier was determined by evaluating vehicular responses specified in the current safety standard, *Manual for Assessing Safety Hardware* (MASH). Nonlinear FE simulations were first carried out on sample designs to obtain the vehicular responses for creating the RBF metamodels, which were then used in the optimization process to replace the expensive FE simulations. An optimal design of the concrete barrier was obtained by the GA and was shown to have improved safety performance over the original design.

1. Introduction

Vehicular crashes on highways usually lead to loss of human lives accompanied by significant social and economic loss. Roadside or median barriers are designed to reduce the risk and injury levels of roadside accidents as they can prevent errant vehicles from colliding with roadside objects such as trees and poles, or running into dangerous areas such as steep slopes or cliffs. A roadside barrier should be designed to be able to safely redirect the vehicles back to the travel lane without getting involved in a second crash with other vehicles.

For decades, full-scale crash testing has been the primary means for evaluating the performance of roadside safety devices such as concrete barriers, W-beam guardrails and cable barriers which are shown in Fig. 1 [1–4]. The first published procedure on how to perform crash tests for assessing safety hardware appeared in 1962 and was entitled "the highway research correlation services circular 482" [5]. In 1993, the report of a project sponsored by the National Cooperative Highway Research Program (NCHRP), known as the NCHRP Report 350, was adopted as the first formal safety standard for roadside safety [6]. Since then, a large number of studies have been conducted using full scale crash testing to evaluate the design of concrete barriers, W-beam guardrails, cable barriers, and other highway safety features [7–19]. A detailed review and analysis of other crash testing works can be found in Ref. [20].

In 2009, the American Association of State Highway & Transportation Officials (AASHTO) adopted a new roadside safety standard to replace the NCHRP Report 350. The new standard, *Manual for Assessing Safety Hardware* (MASH) [21], presents updated guidelines and evaluation criteria for testing highway safety features before installed on U.S. highways. Among the six test levels (TLs) specified by MASH, the TL-3 conditions are the most commonly used for barriers used on freeways. From the NCHRP 350 TL-3 to MASH TL-3, the mass of the small car changes from 820 kg to 1100 kg and the mass of the pickup truck changes from 2000 kg to 2270 kg. In addition, the impact angle changes

* Corresponding author. Tel.: +1 (704) 687 8328; fax: +1 (704) 687 8345.
E-mail address: hfang@uncc.edu (H. Fang).

http://dx.doi.org/10.1016/j.engstruct.2016.02.009
0141-0296/

(a) (b) (c)

Fig. 1. Three typical roadside safety devices [1–4]: (a) concrete barrier; (b) W-beam guardrail; and (c) cable barrier.

from 20 deg to 25 deg for the small car. During the past several years, researchers at Midwest Roadside Safety Facility conducted a number of full-scale crash tests on concrete barriers, W-beam guardrails, and cable barriers under MASH TL-3 conditions [22–28]. Researchers at the Texas Transportation Institute (TTI) also tested concrete barriers, W-beam guardrails, and other highway safety devices under MASH TL-3 conditions [29–34]. In addition, Sheikh et al. at TTI design and tested a concrete bridge rail under MASH TL-4 conditions. The test data were also used to validate the finite element (FE) model of a single unit truck that was used as the test vehicle. Other full-scale testing on roadside hardware devices was also seen in the work by Sennah et al. [35] and Sennah and Khederzadeh [36] in which they tested a PL-3 concrete bridge barrier under MASH TL-5 conditions. Other roadside safety issues such as missing post of longitudinal barriers [37] and evaluation of new containment level guardrail [38] were also investigated using crash testing.

Despite its irreplaceability in determining the compliance of a roadside safety device to the safety standard, full-scale crash testing is practically too expensive to be used in evaluating large matrices of designs. With the development of computer simulation and parallel computational algorithms, it is now popular to perform full-scale FE simulations of vehicular crashes using commercial codes such as LS-DYNA [39]. For roadside safety research, the wide adoption of FE modeling and simulations started in the mid 1990s, as seen in the works by Ray and his colleagues [40–43] and Reid [44–46]. Since then, full-scale FE models of vehicles and roadside safety devices were developed, including small passenger car [47,48], pick-up truck [49–52], single unit truck [53], cable and concrete barriers [54,55]. With the availability of FE models, numerous studies were conducted using numerical simulations to evaluate the performance of various roadside safety devices as well as improving existing numerical models [56–84].

Using numerical simulations, new designs of safety devices can be evaluated timely and efficiently. More importantly, optimum designs can be sought by combining numerical simulations with a mathematical procedure, a method commonly called simulation-based design optimization. Over the years, there have been numerous studies conducted on crashworthiness optimization, at both component and structural levels [85–94]. In simulation-based design optimization (SBDO), the optimization process generally requires a large number of simulations to evaluate the system responses of various designs. Given the high computational cost of crash simulations, a common practice is to use a surrogate model (or metamodel) [95] to replace the expensive simulations in an optimization process. Despite its proofed usefulness, the SBDO has not been widely used in highway safety research for barrier designs. In the recent work by Hou et al. [96], they optimized a concrete barrier's cross-sectional geometry so as to reduce the peak acceleration of the striking vehicle, a small passenger car. Hou et al. [97] also optimized the design of a corrugated guardrail system by changing the rail thickness and post spacing so as to minimize the rail deflection and vehicle acceleration. These two studies clearly demonstrated the applicability of SBDO to roadside barrier designs. However, in the above two studies [96,97], the performance criteria were not those specified in MASH. Additionally, the standard impacting vehicles specified by MASH were not used in these two studies.

In this study, the New Jersey concrete barrier was used to demonstrate a general SBDO methodology for barriers designs in compliance with the MASH safety criteria. The nonlinear FE crash simulations involved both a pickup truck and a small passenger car specified by MASH TL-3 conditions. In the remaining portion of the paper, the barrier design problem is first formulated in mathematical forms for optimization. The FE models of two vehicles are then introduced and model validation using crash test data is presented. The metamodeling technique that is used to create the explicit form of nonlinear vehicular responses is subsequently presented, along with the optimization algorithm and SBDO procedure. Finally, the optimum design of the concrete barrier is sought using the proposed SBDO methodology and compared to the original design, followed by some concluding remarks.

2. Design optimization of roadside barriers

2.1. Safety criteria of roadside barrier design

In the United States, roadside barriers should meet the safety requirements of NCHRP Report 350 [6] (if tested before the issuance of MASH) and MASH [7]. In MASH specifies six test levels for evaluating roadside barriers, with lower test levels targeting lower traffic volume roadways whereas higher test levels for higher traffic volume freeways. The MASH TL-3 conditions, which are the most commonly adopted by state DOTs, are given in Table 1 and employed in this study. It should be noted that 1100C refers to a small passenger car with a mass of 1100 kg and 2270P is for a 2270-kg pickup truck. Fig. 2 illustrates the TL-3 impact conditions and the definition of exit angle (EA) of the vehicle, which is an important criterion for evaluating the safety of roadside barriers.

Table 1
Test matrix for TL-3 in MASH.

Test designation	Vehicle	Impact speed (km/h)	Impact angle (deg)
3-10	1100C	100	25
3-11	2270P	100	25

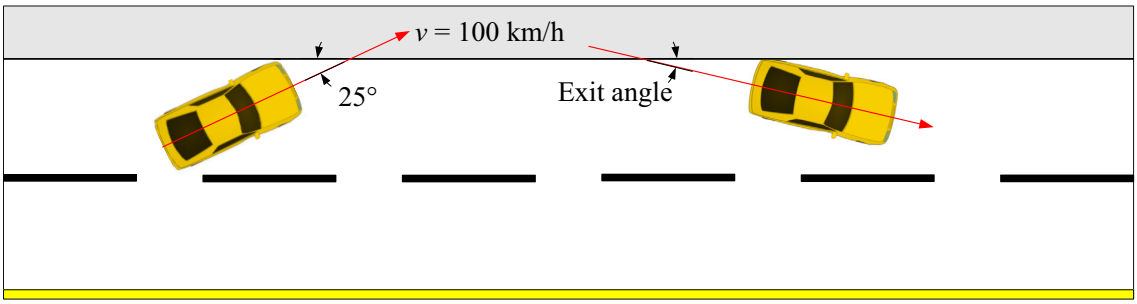

Fig. 2. Illustration of impact conditions and exit angle.

According to MASH, the performance of a barrier system is evaluated on the "structural adequacy of the safety feature", "post-impact behavior of the test vehicle", and "risk of injury to the occupants of the impacting vehicle." For concrete barrier, the "structural adequacy of the safety feature" is usually not a concern at TL-3 conditions. Two important post-impact responses of the vehicle are the vehicle's EA and maximum absolute roll angle (MARA), which relate to the vehicle's safe redirection and rollover, respectively. For occupant injuries, MASH does not have an evaluation criterion that is directly based on occupant responses, because crash test dummy has not been adopted in barrier crash tests. Currently, the evaluation criteria of occupant injury risk are developed based on vehicular responses, e.g., the occupant impact velocity (OIV) and occupant ridedown acceleration (ORA) as specified in MASH.

The OIV is the relative velocity between the hypothetical occupant and the instrument panel. The OIV in the longitudinal or lateral direction can be calculated by

$$\mathrm{OIV}_{x,y} = \int_0^{t_0} a_{x,y}\,dt \tag{1}$$

where $a_{x,y}$ is vehicular acceleration in the longitudinal or lateral direction. In Eq. (1), $t_0 = \min\{t_x, t_y\}$ in which t_x and t_y are the time of free motions of the hypothetical occupant in the longitudinal and lateral directions, respectively, and are determined by solving the following equations.

$$\int_0^{t_x} dt \int_0^{t_x} a_x\,dt = 0.6 \tag{2}$$

$$\int_0^{t_y} dt \int_0^{t_y} a_y\,dt = 0.3 \tag{3}$$

The ORA is the largest 10-ms average accelerations of the hypothetical occupant during the subsequent ridedown after time instant t_0. The acceptable maximum OIV and ORA specified in MASH are 12.2 m/s and of 20.49 g, respectively, and the preferred maximum OIV and ORA are 9.1 m/s and 15.0 g, respectively. In this study, the limits for OIV and ORA were set to 12.2 m/s and 20.49 g, respectively.

2.2. Optimization formulation of barrier design problem

In general, a standard optimization problem can be written as follows

$$\begin{aligned} &\min\ f(\mathbf{x}) \\ &\text{s.t. } g_i(\mathbf{x}) \leqslant 0, \quad i = 1, \cdots, N_g \\ &\quad \mathbf{x}^{\mathrm{L}} \leqslant \mathbf{x} \leqslant \mathbf{x}^{\mathrm{U}}, \quad \mathbf{x} = [x_1, \cdots, x_n] \end{aligned} \tag{4}$$

where $\mathbf{x}$ is an n-dimensional vector of design variables, $\mathbf{x}^{\mathrm{L}}$ and $\mathbf{x}^{\mathrm{U}}$ are the lower and upper bounds, respectively, of $\mathbf{x}$, $f(\mathbf{x})$ is the objective, and $g_i(\mathbf{x})$ $(i = 1, 2, \ldots, N_g)$ are the inequality constraints. For a barrier design, one of the safety criteria (i.e. OIV, ORA, MARA, EA) could be selected as the objective function and the rest of them as the constraints with MASH specified limit values.

3. Numerical simulation of roadside crash

3.1. The FE models of vehicles and concrete barrier

In this study, a 1996 Dodge Neon passenger car and a 2007 Chevy Silverado pickup truck were selected as the MASH TL-3 test vehicles. The FE models of these two vehicles, as shown in Fig. 3, were originally developed at the National Crash Analysis Center (NCAC) and their vehicular masses met the TL-3 requirement of 1100 kg and 2270 kg, respectively. The FE models of the two vehicles were initially validated by full frontal impact tests and other NCAC-developed validation exercises [98–102]. These validations provided a good basis for using these vehicle models for the roadside barrier impact simulations in this study.

The New Jersey concrete barrier, which is commonly referred to as Jersey barrier as shown in Fig. 4a, is the most widely used concrete barrier in the U.S. The FE model of the Jersey barrier used in this study was also developed at NCAC and is shown in Fig. 4b. Fig. 5 shows the original cross-sectional geometries of the Jersey barrier for this study in which x_1 = 51 mm and x_2 = 178 mm. In this study, we mainly investigate the design variables which control the geometry shape of the vehicle-barrier impact face of the concrete barrier. Thus, the height and the bottom width of the concrete barrier were not treated as variables. The two design parameters, x_1 and x_2, largely control the shape of the concrete barrier and thus were chosen as the design variables in the optimization work of this study. To ensure the vehicle did not reach the end of the barrier during the course of impact, the length of the barrier was set to 20 m. Since concrete barriers generally do not deform even under severe crash conditions, the rigid material (MAT20 in LS-DYNA) was used for the concrete barrier in the FE model. Some previous studies [55,82,96] demonstrate that modeling the barrier as completely rigid is a commonly accepted approach. The bottom of the barrier was fixed to prevent displacements during the impact, as is the case of an in-service concrete barrier. The FE models of the barrier systems which were constructed using LS-DYNA software were given in Fig. 6.

3.2. Validation of the FE models

Before used in barrier optimization of this study, the FE models were validated by comparing simulation results with full-scale crash tests from the work by Marzougui et al. [82]. It should be noted that the 1100C vehicle used in the crash tests was a 2010 Toyota Yaris and had a very similar profile and mass to the Dodge Neon. Figs. 7 and 8 show the front views of simulated vehicular responses compared to test data for the 1100C and 2270P vehicles,

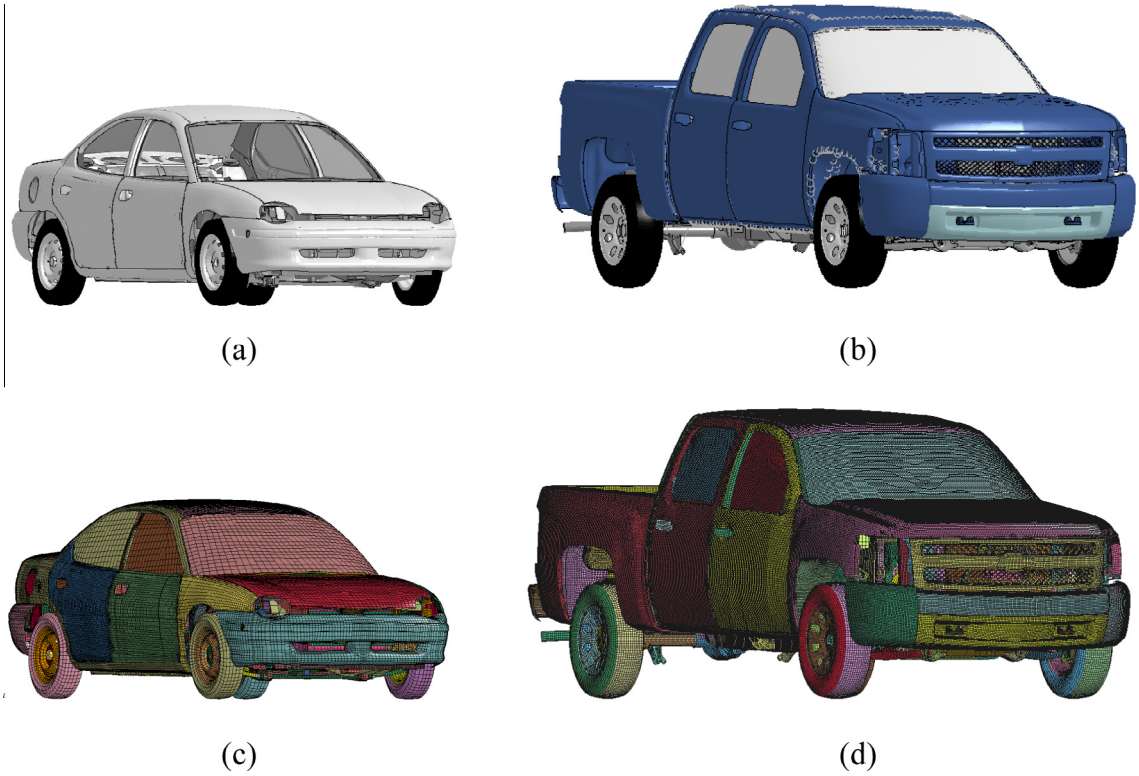

Fig. 3. The FE models of a small passenger car (1100C) and a pickup truck (2270P): (a) 1996 Dodge Neon without mesh; (b) 2007 Chevy Silverado without mesh; (c) 1996 Dodge Neon with mesh; and (d) 2007 Chevy Silverado with mesh.

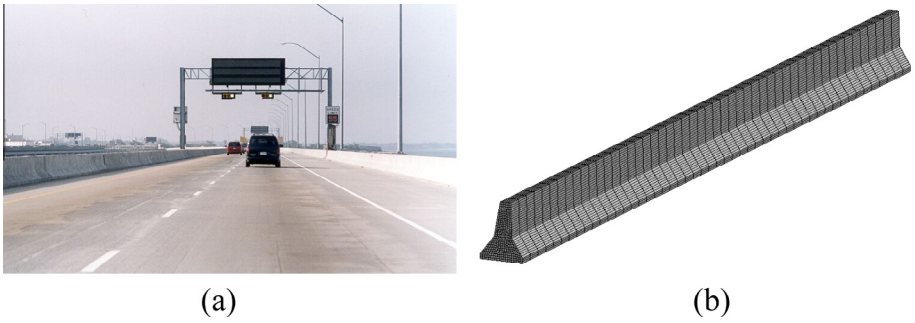

Fig. 4. The New Jersey concrete barrier: (a) an in-service system; and (b) the FE model.

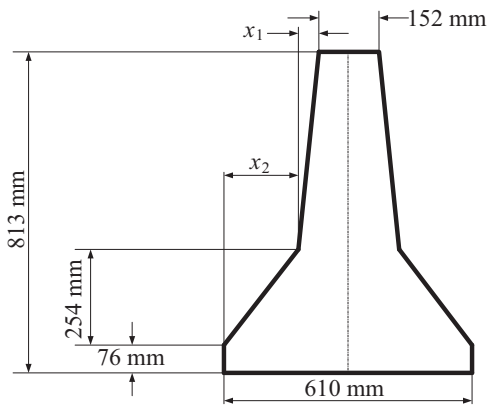

Fig. 5. The cross-sectional sizes of New Jersey safety-shape barrier.

respectively, while impacting into a Jersey barrier. It was observed from the comparisons in Figs. 7 and 8 that both models produced similar vehicular responses to those of their respective test vehicle. The comparisons of yaw and roll angles between numerical simulations and test data for both vehicles were given in Figs. 9 and 10. It can be seen that the FE simulation results are in good agreement with test data. Based on these comparisons, the FE models were deemed suitable for simulating the roadside impacts to evaluate the performance of the Jersey barrier.

4. Metamodeling-based optimization framework

For many engineering problems, the system responses are often implicit functions of the design variables, e.g., vehicle's exit angle in relation to the cross-sectional geometry in the case of concrete barrier design. Although the responses corresponding to each

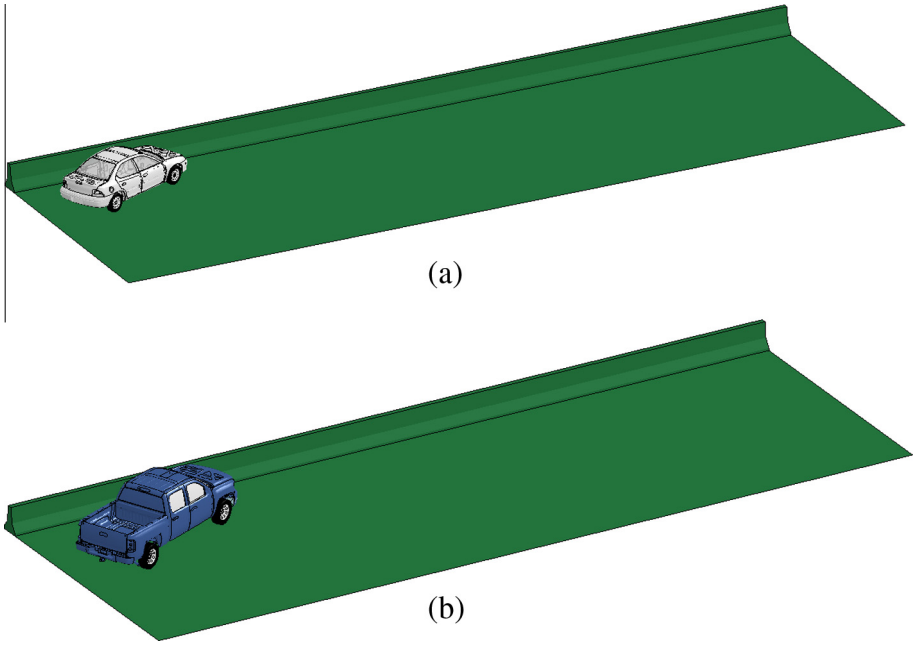

Fig. 6. The FE models of the whole barrier system: (a) Neon; and (b) Silverado.

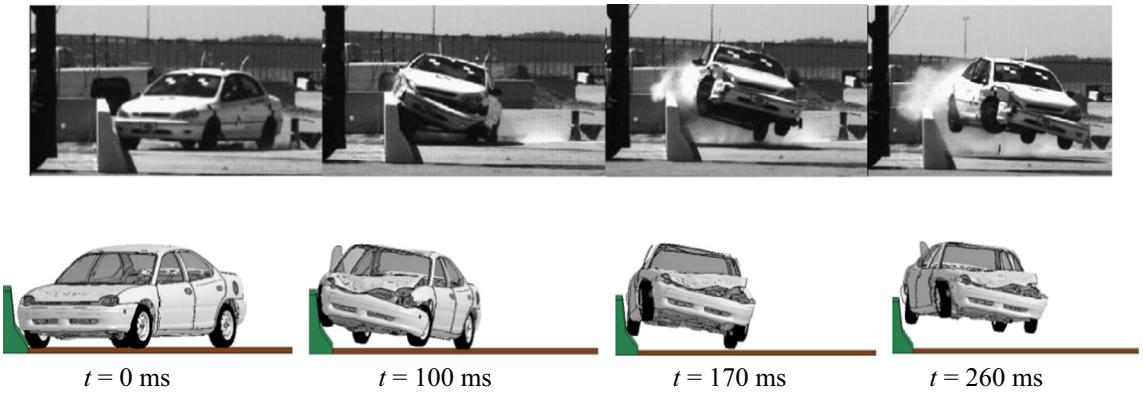

Fig. 7. Visual comparison of crash test and simulation results for 1100C.

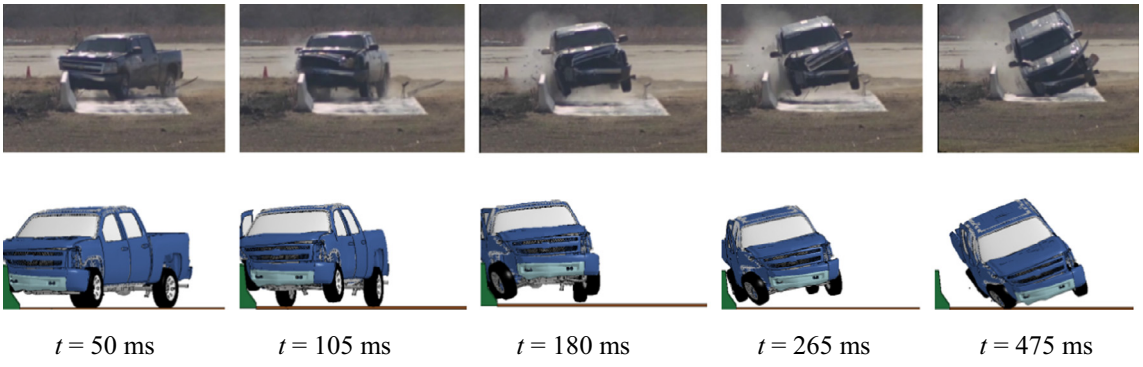

Fig. 8. Visual comparison of crash test and simulation results for 2270P.

design can be evaluated using numerical tools such as FE simulations, the large number of simulation required by the optimization process makes it very inefficient and impractical to directly use FE simulations. To this end, a metamodeling-based optimization method, specifically based on radial basis functions (RBFs) [103] was proposed so that an approximate function in explicit form could be created for implicit each response function. An RBF meta-model was created using the responses (calculated by FE simulations) on some preselected points (called design points or samples) and then used in the subsequent optimization procedure.

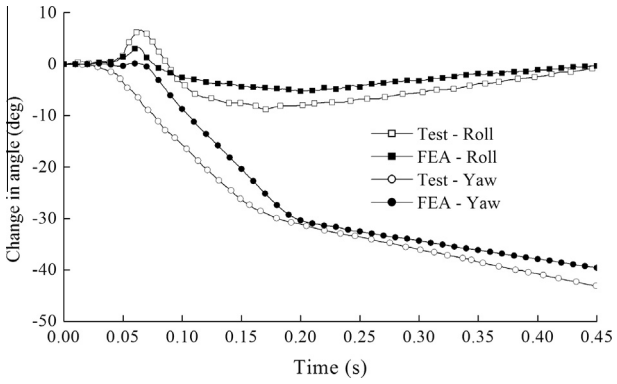

Fig. 9. Comparison of yaw and roll angles between test and FE analysis for 1100C.

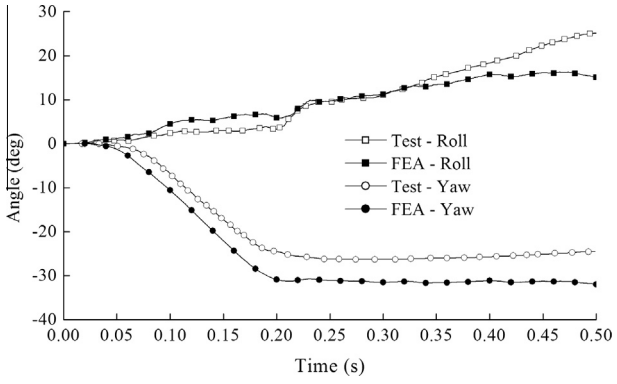

Fig. 10. Comparison of yaw and roll angles between test and FE analysis for 2270P.

4.1. Design of experiment (DOE)

A DOE method provides a systematic, and often efficient, means of selecting the samples that can give a reasonably good representation of the design space. Commonly used DOE methods include full factorial design (FFD), central composite design, Latin hypercube design, and Taguchi orthogonal array [104–106]. Each DOE method has its own advantages and disadvantages. Among the many different DOE methods, the FFD is often the preferred method for its advantage of uniformity when the number of design variables is small (i.e., three or less). In this study, we employed FFD to generate the initial samples, which were used to create the RBF models for design optimization.

4.2. Metamodeling with radial basis functions (RBFs)

RBF is one of the multi-dimensional interpolation methods and has been widely used for approximating engineering system responses involving expensive numerical simulations. For an unknown, true response $y(\mathbf{x})$, the RBF metamodel has the following mathematical form

$$\hat{y}_{\mathrm{RBF}}(\mathbf{x}) = \sum_{i=1}^{n} r_i \phi_i(\|\mathbf{x} - \mathbf{x}_i\|) \tag{5}$$

where n is the number of samples, $\mathbf{x}$ is an n-dimensional vector of variables, $\mathbf{x}_i$ is the vector of design variables at the ith sampling point, ϕ is the basis function, $\|\mathbf{x} - \mathbf{x}_i\|$ is the Euclidean distance, and r_i is the coefficient of the ith basis function. Therefore, an RBF is actually a linear combination of n basis functions with weighted coefficients. Some of the most commonly used basis functions are summarized in Table 2 [21]. In Table 2, d is the Euclidean distance and c is a user-defined constant.

Table 2
Commonly used basis functions.

Basis function	Equation
Thin plate	$\phi(d) = d^2 \ln(cd^2)$
Gaussian	$\phi(d) = \exp(-cd^2)$
Multi-quadric	$\phi(d) = \sqrt{c^2 + d^2}$
Inverse multi-quadric	$\phi(d) = 1/\sqrt{c^2 + d^2}$

By replacing $\mathbf{x}$ and $\hat{y}_{\mathrm{RBF}}(\mathbf{x})$ in Eq. (5) with n vectors of design variables and their corresponding true function values at the sampling points, we can obtain the following n equations

$$\begin{aligned} y_1 &= \sum_{i=1}^{n} r_i \phi_i(\|x_1 - x_i\|) \\ y_2 &= \sum_{i=1}^{n} r_i \phi_i(\|x_2 - x_i\|) \\ &\cdots \\ y_n &= \sum_{i=1}^{n} r_i \phi_i(\|x_n - x_i\|) \end{aligned} \tag{6}$$

The matrix form of Eq. (6) is

$$\mathbf{Y} = \mathbf{AR} \tag{7}$$

where $\mathbf{Y} = [y_1, y_2, \ldots, y_n]^{\mathrm{T}}$, y_i $(i = 1, 2, \ldots, n)$ is the corresponding true function value, $A_{i,j} = \phi(\|x_i - x_j\|)$ $(i = 1, 2, \ldots, n, j = 1, 2, \ldots, n)$, and $\mathbf{R} = [r_1, r_2, \ldots, r_n]^{\mathrm{T}}$. Therefore, the coefficient matrix $\mathbf{R}$ can be determined by

$$\mathbf{R} = \mathbf{A}^{-1}\mathbf{Y} \tag{8}$$

The accuracy of an RBF model can be evaluated using the relative error (RE) between the FE analysis results $y(\mathbf{x})$ and the predicted values by the RBF model $\hat{y}(\mathbf{x})$ at some off-design points, given as

$$\mathrm{RE} = \frac{\hat{y}(\mathbf{x}) - y(\mathbf{x})}{y(\mathbf{x})} \tag{9}$$

In addition, the accuracy of the RBF model can be evaluated using the root mean square error (RMSE) and the maximum absolute error (MAE), respectively, which are written as

$$\mathrm{RMSE} = \sqrt{\frac{\mathrm{SS_E}}{k}} \tag{10}$$

$$\mathrm{MAE} = \max|y_i - \hat{y}_i|, \quad i = 1, 2, \cdots, n \tag{11}$$

where k is the number of validation points. The MAE is used to gauge the local accuracy of the model, while the RSME is used to gauge the overall accuracy of the model. The smaller the values of RSME and MAE, the more accurate the RBF models are. In Eq. (10), the SSE is the sum of squared errors, which can be calculated as

$$\mathrm{SSE} = \sum_{i=1}^{n} (y_i - \hat{y}_i)^2 \tag{12}$$

According to the above theory, an RBF modeling procedure was written using matlab language and was used in the following RBF-based optimization.

4.3. Genetic algorithm (GA)

A GA is a popular global optimization method that was originated from the mechanisms of natural evolution and genetic

principles and was inspired by Darwin's theory about evolution. A GA is superior to many traditional optimization algorithms because of its capability of avoiding trapping in local optima for searching an optimum [22]. A GA is started with a set of solutions (represented by chromosomes) called a population. Solutions from one population are taken and used to form a new population. This is motivated by a hope, that the new population will be better than the old one. Solutions which are selected to form new solutions (offspring) are selected according to their fitness – the more suitable they are the more chances they have to reproduce. This is repeated until some criteria (e.g. number of populations or improvement of the best solution) are satisfied [23]. A GA is easy to understand and can solve multi-dimensional, non-differential, non-continuous, and even non-parametrical problems. In this study, a GA procedure in matlab was used to solve the barrier optimization problem.

4.4. Procedure of RBF-based optimization method

The flowchart of this RBF-based optimization method was provided in Fig. 11 and more detailed description is given as follows.

STEP 1: Define the initial parameters such as the number of initial samples, the numbers of objectives and variables, and the ranges of design variables.
STEP 2: Generate initial samples based on the FFD DOE method.
STEP 3: Evaluate the objective and constraint function values at the initial sampling points using nonlinear FE code LS-DYNA. Thus, this is a time-consuming step.
STEP 4: With the simulation results obtained in *STEP 3*, the RBF models can be constructed to establish the relationship between the objective and constraint functions and the design variables. In this study, RBF models are constructed according to Section 4.2. If the RBF models are accurate enough, go to *STEP 5*; otherwise go to *STEP 7*.
STEP 5: Based on the metamodels obtained in *STEP 4*, the optimization is implemented using GA.
STEP 6: The optimal solution of the optimization problem is obtained. Stop the optimization process.
STEP 7: Generate K additional samples in the design space. The objective and constraint function values of the K additional samples are calculated using numerical simulations.
STEP 8: The K new samples are added to the design samples. Go back to *STEP 4*. The RBF models of objective and constraint functions can be reconstructed according to all available design samples.

5. Design optimization of the concrete barrier

5.1. Sensitivity analysis of crash responses

Using the validated FE models, different designs of the concrete barrier were evaluated. In this study, there were two design variables, denoted as x_1 and x_2 and illustrated in Fig. 5. The ranges of x_1 and x_2 were set as 0–76 mm (3 in.) and 0–203 mm (8 in.), respectively. The 25 sampling points generated by a full factorial design are illustrated in Fig. 12 and used for each vehicle to investigate the performance of the concrete barrier.

The vehicular responses of the two test vehicles were obtained using numerical simulations. The OIV, ORA, MARA, and EA values of these 25 cases for the 1100C and 2270P vehicles are shown in Figs. 13–16. The limits of MASH safety criteria on these safety parameters are also plotted in Figs. 13–16. It can be seen that the OIV, ORA and EA were all below the limits; only the MARA exceeded the MASH limit. From Figs. 13–16, it was also observed that the variations of the OIV and EA of both the 1100C and

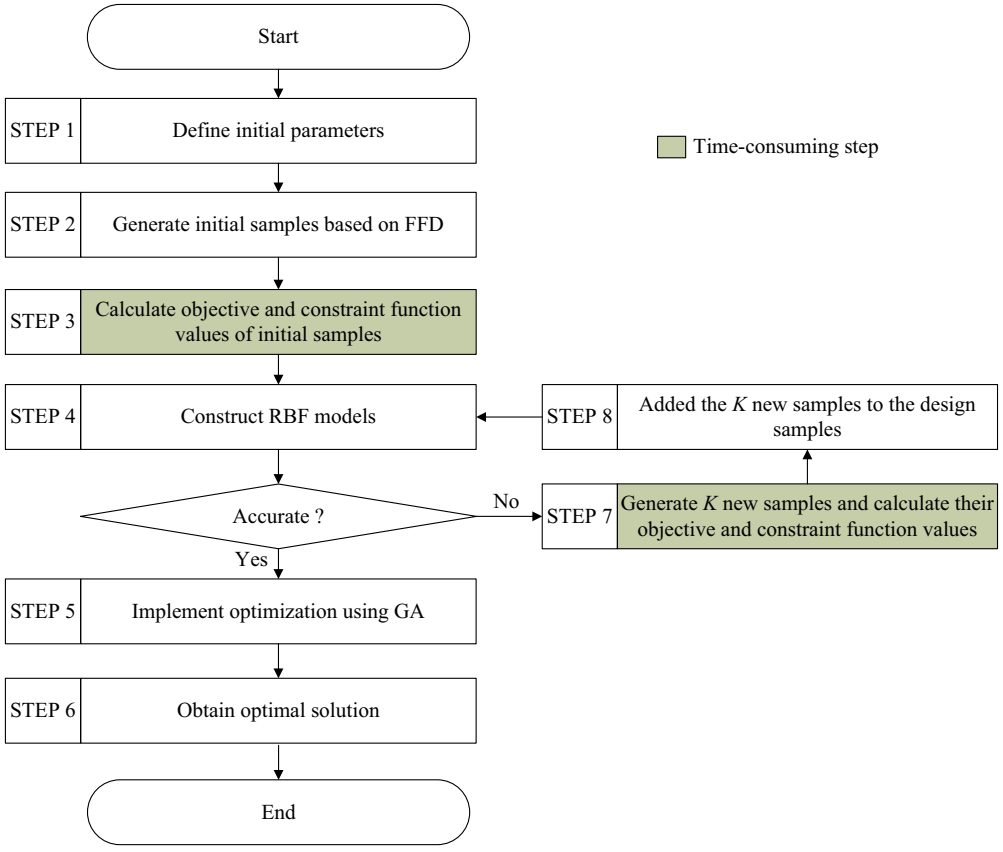

Fig. 11. Flowchart of RBF-based optimization method.

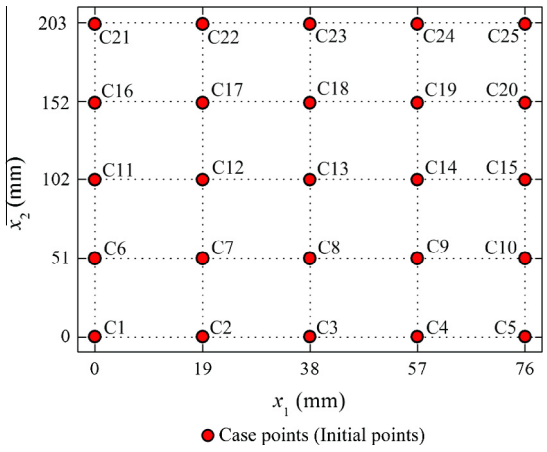

Fig. 12. Illustration of the 25 investigated cases.

2270P vehicles were relatively small, while the variations of the ORA and MARA were relatively large. In other words, the safety criteria of the OIV and EA were not very sensitive to the design changes, while the ORA and MARA were sensitive to the change of design variables.

5.2. Formulation of the optimization problem

The MARA was found to be sensitive to design changes and a large MARA suggested a high risk of vehicle rollover. Moreover, the MARA values were large in some cases, most of which were with the 2270P vehicle. For a barrier design, a small MARA value is preferred to reduce the rollover risk of vehicles; thus, the MARA of the 2270P vehicle was chosen as the objective to be minimized in the optimization problem. The MARA of the 1100C vehicle was set as a constraint with a limit of 10 deg angle. Although the other safety criteria (i.e. OIV, ORA and EA) were all satisfied in the 25 design cases, they should be included in the optimization formulation as design constraints so that the optimum designs (unknown before optimization) would not violate these criteria. According to MASH, the limits of OIV and ORA were 12.2 m/s and 20.49 g, respectively. The limit value of EA was calculated using the definition of the exit box criteria in MASH. For the 1100C and 2270P vehicles, the limits of EAs were calculated as 15.77° and 16.92°, respectively. In this study, the limit of MARA of the 1100C vehicle was set as 10°. For this concrete design problem, the optimization problem in Eq. (4) can be formulated as

$$\begin{aligned} \text{Min.}\quad & \text{MARA}^{\text{P}} \\ \text{s.t.}\quad & \text{OIV}^{\text{C}}_{\max} \leqslant 12.2 \\ & \text{OIV}^{\text{P}}_{\max} \leqslant 12.2 \\ & \text{ORA}^{\text{C}}_{\max} \leqslant 20.49 \\ & \text{ORA}^{\text{P}}_{\max} \leqslant 20.49 \\ & \text{EA}^{\text{C}} \leqslant 15.77 \\ & \text{EA}^{\text{P}} \leqslant 16.92 \\ & \text{MARA}^{\text{C}} \leqslant 10 \\ & 0 \leqslant x_1 \leqslant 76 \\ & 0 \leqslant x_2 \leqslant 203 \end{aligned} \tag{13}$$

where the superscripts 'P' and 'C' denote the 2270P and 1100C vehicles, respectively. In order to solve the problem of Eq. (13), the RBF-based optimization method described in Section 4.4 was used. First, the RBF models of objective and constraint functions

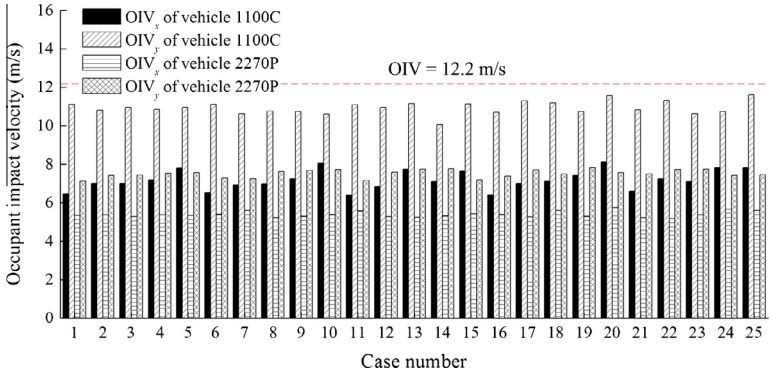

Fig. 13. OIVs of the 25 investigated cases.

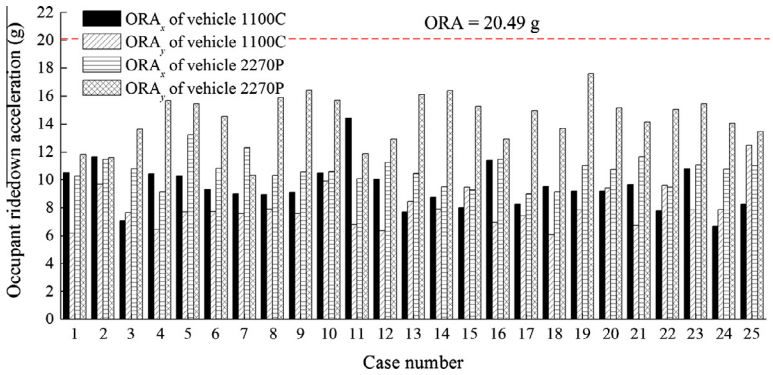

Fig. 14. ORAs of the 25 investigated cases.

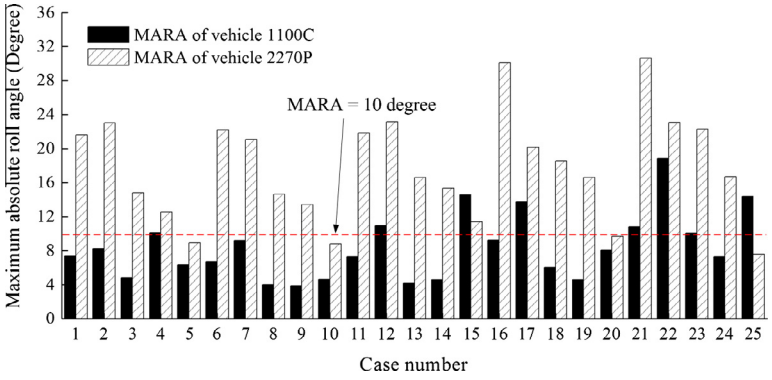

Fig. 15. MARAs of the 25 investigated cases.

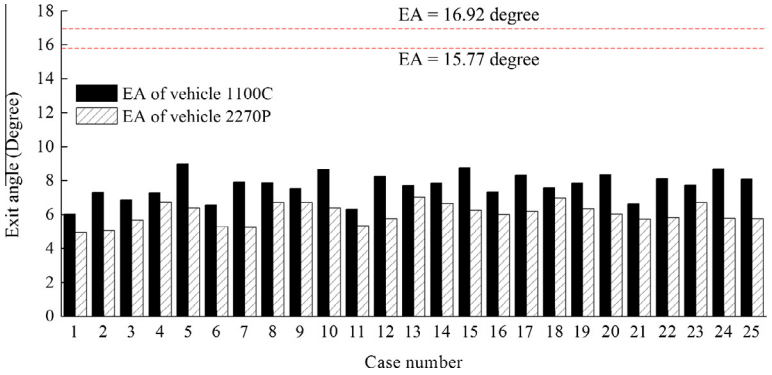

Fig. 16. EAs of the 25 investigated cases.

Table 3
First validation samples.

Vehicle	Sample no.	x_1 (mm)	x_2 (mm)	OIV_x (m/s)	OIV_y (m/s)	ORA_x (g)	ORA_y (g)	MARA (deg)	EA (deg)
1100C	1	25	68	6.66	11.07	11.18	8.30	12.18	6.42
	2	51	68	11.36	6.74	10.17	6.74	12.41	7.07
	3	25	135	7.07	10.90	10.57	7.23	3.89	7.17
	4	51	135	7.07	11.04	9.84	7.70	4.01	8.00
2270P	1	25	68	5.27	7.70	12.14	12.60	19.42	6.12
	2	51	68	5.29	7.74	9.17	14.74	18.07	6.05
	3	25	135	5.55	7.64	10.05	15.19	14.11	6.78
	4	51	135	5.31	7.92	9.79	16.19	17.58	6.78

Table 4
Second validation samples.

Vehicle	Sample no.	x_1 (mm)	x_2 (mm)	OIV_x (m/s)	OIV_y (m/s)	ORA_x (g)	ORA_y (g)	MARA (deg)	EA (deg)
1100C	1	38	68	7.08	11.13	9.16	8.73	10.75	6.90
	2	38	135	7.06	11.00	10.40	6.65	4.10	7.79
	3	25	102	7.44	11.11	7.14	6.38	4.87	7.64
	4	51	102	7.07	11.06	7.85	6.36	5.68	7.19
2270P	1	38	68	5.38	7.76	9.96	13.68	19.33	5.55
	2	38	135	5.34	7.85	9.65	15.56	15.95	6.71
	3	25	102	5.28	7.80	9.70	15.20	15.30	6.73
	4	51	102	5.32	7.91	11.27	14.94	16.78	6.89

were established. In the process of establishing the RBF models, a total of 25 initial design samples (i.e. 25 samples for each vehicle as shown in Fig. 12) were generated using a 5×5 full factorial design. The responses (i.e. safety criteria) of these design samples (Figs. 13–16) were used to create the metamodels of the MARA, OIV, ORA, and EA.

Table 5
Accuracies of RBF metamodels of MARAs.

	No. of samples	Vehicle	RMSE	MAE	RE [min, max] (%)
Initial RBF models	25	1100C	2.4328	4.4254	[−7.69, 57.07]
		2270P	0.9828	1.8322	[−9.21, 3.91]
Updated RBF models	29	1100C	0.4574	0.7615	[−5.64, 7.62]
		2270P	0.7691	1.1040	[−6.17, 0.92]

5.3. Numerical results

Before using the RBF models in optimization, the accuracy of the models, particularly for the $MARA^P$ and $MARA^C$, were evaluated using four additional samples that were randomly generated. In the metamodel-based optimization method, the accuracy of the metamodel affects the accuracy of the optimal result because the objective function values are calculated using the metamodel. Generally, for the complicated engineering problems, the error of the metamodel should be less than 5–10%. The values of MARA and other criteria at the four validation points were obtained using FE simulation results and given in Table 3. The accuracy the initial RBF models of MARAs were not satisfactory, as seen from the large relative errors in Table 5. To improve the accuracy of these RBF models, the four validation samples were added to the initial design samples to establish new RBF models using a total of 29 design samples. The updated RBF models were validated using a second set of four additional samples on which the FE simulation results of the criteria were obtained and shown in Table 4. The updated RBF models were shown to have less than 8% of relative errors based on the results given in Table 5, and thus were considered acceptable for the engineering design of this study.

The optimization problem in Eq. (13) was solved using RBF-based optimization method and the optimal design of the concrete barrier was obtained. The cross section of the optimal concrete barrier is shown in Fig. 17 along with the original design. The safety criteria corresponding to the original and optimal design are given in Table 6.

It was observed from the results in Table 6 that the optimal design resulted in a significant reduction on the MARA of the 2270P vehicle, and the MARA of the 1100C vehicle was also reduced. The other safety criteria, the OIV, ORA, and EA, were all within the MASH limits and there were no significant change from the original to the optimal design. Fig. 18 shows the positions of the 1100C and 2270P vehicles at instants of the maximum roll angles for the optimal and original designs. It can be seen from the vehicle postures that the optimal design resulted in more stability for the pickup truck than the original design, an indication of the improved safety by the optimal design.

Fig. 19 shows the top views of vehicle redirection for both of the 1100C and 2270P vehicles impacting the optimal concrete barrier. It can be seen that both vehicles were smoothly redirected and stayed mostly upright during the impact. Considering the vehicular responses of the two vehicles on the optimal concrete barrier, it can be concluded that the optimal concrete barrier meets the safety requirements specified by MASH. It should be noted that the improvement of the optimal design over the original design was not significant except for the MARA of the 2270P vehicle. This was because the original design of the concrete barrier had been empirically improved by engineers over the years of its usage. Nevertheless, the RBF-based design optimization method employed in this study was shown to be effective and efficient in roadside

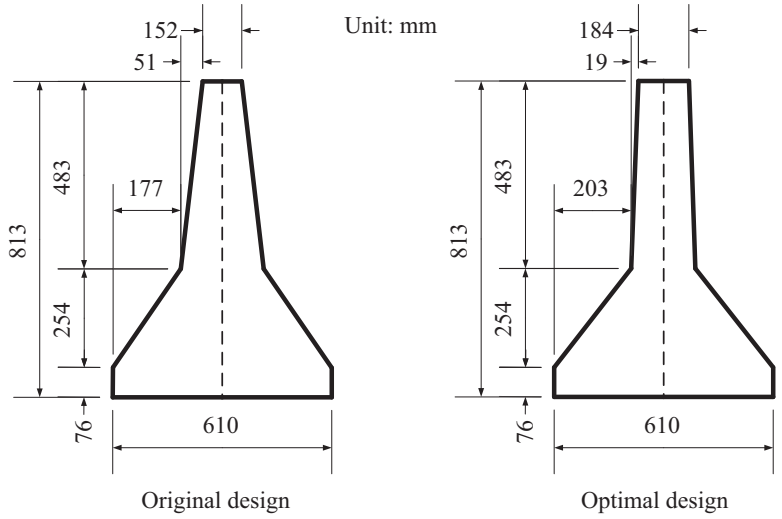

Fig. 17. Cross sections of the original and optimal designs.

Table 6
Responses of original and optimal designs.

	x_1 (mm)	x_2 (mm)	Vehicle	OIV_x (m/s)	OIV_y (m/s)	ORA_x (g)	ORA_y (g)	MARA (deg)	EA (deg)
Original design	51	177	1100C	7.03	10.79	7.76	8.78	5.28	8.07
			2270P	5.18	7.70	10.78	15.96	14.74	6.24
Optimal design	19	203	1100C	8.08	10.61	10.50	9.90	4.67	8.67
			2270P	5.38	7.74	10.61	15.71	8.80	6.38

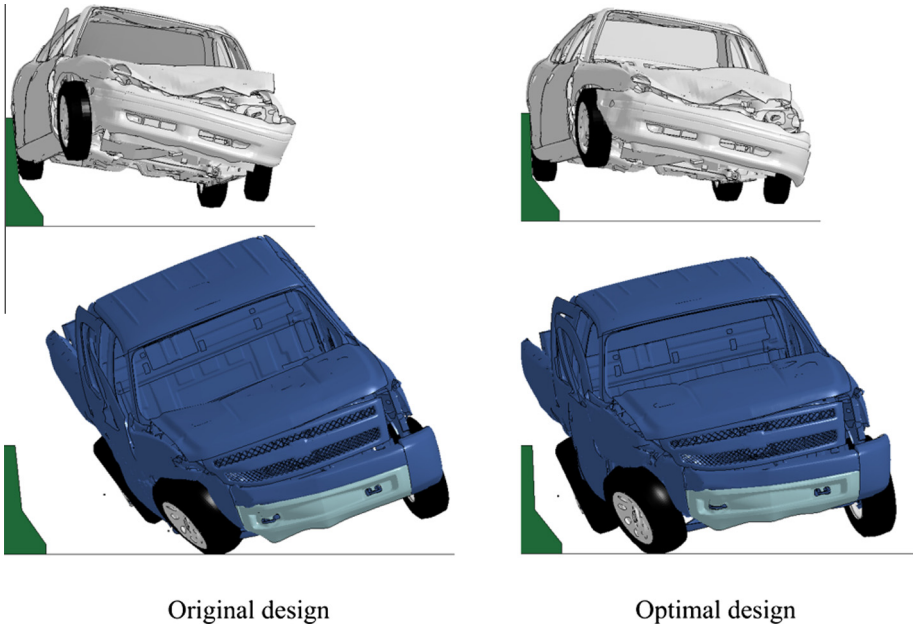

Fig. 18. The vehicle postures when the maximum roll angle existed.

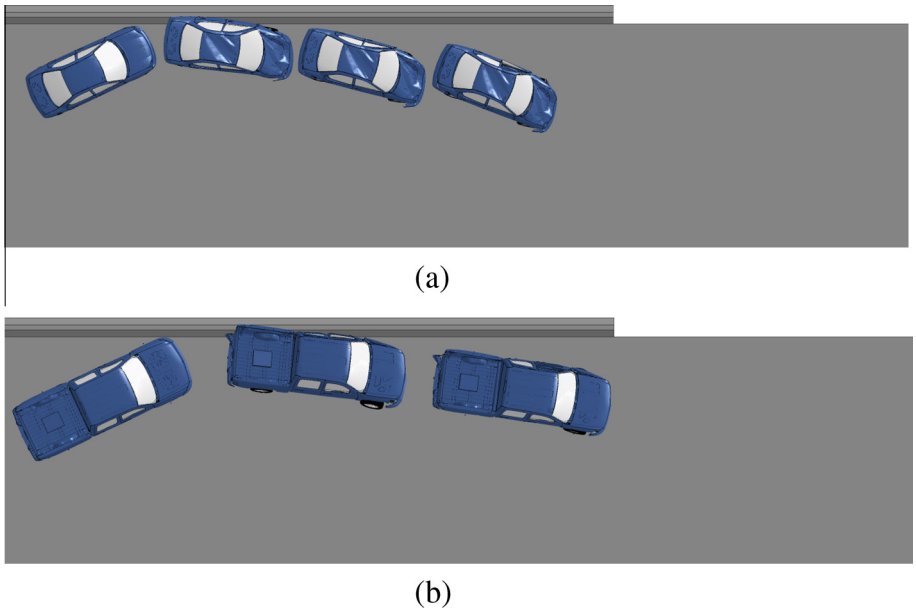

Fig. 19. Redirection of the two vehicles by the optimal concrete barrier design: (a) 1100C: Neon sedan; and (b) 2270P: Silverado pickup truck.

designs and could be used to design and/or optimize other barrier systems for a continuous improvement of roadside safety.

6. Conclusions

In this study, a highway concrete barrier was optimized to improve its performance in redirecting a striking vehicle based on the TL-3 safety requirements specified by Manual for Assessing Safety Hardware (MASH). The finite element (FE) models of two vehicles, a small passenger car and a pickup truck, were created and validated using full-scale crash test data. FE simulations of vehicles impacting the concrete barrier were performed to obtain the vehicular responses used for safety evaluation. To reduce the computational cost of optimization that required a large number of simulations, an RBF-based metamodeling methodology was employed to create surrogate models that were used to replace the expensive FE simulations in optimization. Based on a sensitivity analysis of the vehicular responses, the maximum absolute roll angle (MARA) of the pickup truck was chosen as the objective function to be minimized, and other MASH specified responses such as occupant impact velocity and occupant ridedown acceleration were used as the constraints.

Using the NSGA-II, an optimal design, i.e., the cross-section geometry of the concrete barrier, was obtained and validated by FE simulations. The optimal design was shown to significantly reduce the MARA of the pickup truck compared to the original design (from 14.74 to 8.80 deg), while the MARA of the passenger

car and other safety parameters for both vehicles did not have significant changes. The optimization results indicated the validity and applicability of the metamodeling-based optimization methodology in this study. It should be noted that the improvement of the optimal design over the original design was not significant except for the MARA of the pickup truck. This was because the original design of the concrete barrier had been empirically improved by engineers over the years of its usage. Nevertheless, the RBF-based design optimization method employed in this study was shown to be effective and efficient in roadside designs and could be used to design and/or optimize other barrier systems for a continuous improvement of transportation safety.

References

[1] https://en.wikipedia.org/wiki/File:Concrete-step-barrier-M18.jpg.
[2] http://i01.i.aliimg.com/img/pb/933/001/296/296001933_554.jpg.
[3] http://media.mlive.com/kzgazette_impact/photo/9260974-large.jpg.
[4] http://www.mainlinefence.com/gallery/category/guard-rails.
[5] Committee on Guardrails and Guide Posts. Proposed full-scale testing procedures for guardrails. Highway research correlation service circular 482. Washington (DC): Highway Research Board; 1962.
[6] Ross Jr HE, Sicking DL, Zimmer RA, Michie JD. Recommended procedures for the safety performance evaluation of highway features. NCHRP report 350. Washington (DC): Transportation Research Board, National Research Council; 1993.
[7] Reid JD, Sicking DL, Faller RK, Pfeifer B. Development of a new guardrail system. Transp Res Rec 1997;1599(1):72–80.
[8] Plaxico CA, Ray MH, Hiranmayee K. Impact performance of the G4(1W) and G4(2W) guardrail systems: comparison under NCHRP report 350 test 3-11 conditions. Transp Res Rec 2000;1720:7–18.
[9] Ray M, Engstrand K, Plaxico C, McGinnis R. Improvements to the weak-post W-beam guardrail. Transp Res Rec 2001;1743(1):88–96.
[10] Sicking DL, Reid JD, Rohde JR. Development of the midwest guardrail system. Transp Res Rec 2002;1797:44–52.
[11] Consolazio GR, Chung JH, Gurley KR. Impact simulation and full scale crash testing of a low profile concrete work zone barrier. Comput Struct 2003;81:1359–74.
[12] Faller RK, Polivka KA, Kuipers BD, Bielenberg RW, Reid JD, Rohde JR, Sicking DL. Midwest guardrail system for standard and special applications. Transp Res Rec 2004;1890(1):19–33.
[13] Atahan AO, Cansiz Ö. Improvements to G4 (RW) strong-post round-wood, W-beam guardrail system. J Transp Eng 2005;131(1):63–73.
[14] Ren Z, Vesenjak M. Computational and experimental crash analysis of the road safety barrier. Eng Fail Anal 2005;12:963–73.
[15] Buth CE, Bullard DL, Menges WL. NCHRP report 350 test 3-11 of the long-span guardrail with 5.7 m clear span and nested W-beams over 11.4 m. Report 405160-1-1. Texas: Texas Transportation Institute; 2006.
[16] Plaxico CA, Kennedy JC, Miele CR. Development of an NCHRP report 350 TL-3 New Jersey shape 50-inch portable concrete barrier. Final report FHWA/OH-2006/16. Ohio Department of Transportation; 2006.
[17] Davids WG, Botting JK, Peterson M. Development and structural testing of a composite-reinforced timber highway guardrail. Constr Build Mater 2006;20:733–43.
[18] Faller R, Sicking D, Bielenberg R, Rohde J, Polivka K, Reid J. Performance of steel-post, W-beam guardrail systems. Transp Res Rec 2007;2025:18–33.
[19] Faller R, Reid J, Kretschmann D, Hascall J, Sicking D. Midwest guardrail system with round timber posts. Transp Res Rec 2009;2120:47–59.
[20] Soltani M, Moghaddam TB, Karim MR, Sulong NH. The safety performance of guardrail systems: review and analysis of crash tests data. Int J Crashworthiness 2013;18:530–43.
[21] AASHTO MASH-1. Manual for assessing safety hardware (MASH). 1st ed. Washington (DC): American Association of State Highway Transportation Officials; 2009
[22] Wiebelhaus MJ, Terpsma RJ, Lechtenberg KA, Faller RK, Sicking DL, Bielenberg RW, Reid JD, Rohde JR. Development of a temporary concrete barrier to permanent concrete median barrier approach transition. Report TRP-03-208-10. Lincoln (NE): Midwest Roadside Safety Facility (MwRSF); 2010.
[23] Rosenbaugh SK, Lechtenberg KA, Faller RK, Sicking DL, Bielenberg RW, Reid JD. Development of the MGS approach guardrail transition using standardized steel posts. Report TRP-03-210-10. Lincoln (NE): Midwest Roadside Safety Facility (MwRSF); 2010.
[24] Wiebelhaus MJ, Johnson EA, Sicking DL, Faller RK, Lechtenberg KA, Rohde JR, Bielenberg RW, Reid JD, Rosenbaugh SK. Phase I development of a non-proprietary, four-cable, high tension median barrier. Report TRP-03-213-11. Lincoln (NE): Midwest Roadside Safety Facility (MwRSF); 2011.
[25] Schmidt JD, Sicking DL, Faller RK, Lechtenberg KA, Bielenberg RW, Reid JD, Rosenbaugh SK. Phase II development of a non-proprietary, four-cable, high tension median barrier. Report TRP-03-253-12. Lincoln (NE): Midwest Roadside Safety Facility (MwRSF); 2012.
[26] Stolle CJ, Lechtenberg KA, Reid JD, Faller RK, Bielenberg RW, Rosenbaugh SK, Sicking DL, Johnson EA. Determination of the maximum MGS mounting height – phase I crash testing. Report TRP-03-255-12. Lincoln (NE): Midwest Roadside Safety Facility (MwRSF); 2012.
[27] Julin RD, Reid JD, Faller RK, Mongiardini M. Determination of the maximum MGS mounting height – phase II detailed analysis using LS-DYNA. Report TRP-03-274-12. Lincoln (NE): Midwest Roadside Safety Facility (MwRSF); 2012.
[28] Gutierrez DA, Lechtenberg KA, Bielenberg RW, Faller RK, Reid JD, Sicking DL. Midwest guardrail system (MGS) with southern yellow pine posts. Report TRP-03-272-13. Lincoln (NE): Midwest Roadside Safety Facility (MwRSF); 2013.
[29] Williams WF, Menges WL. MASH test 3-11 of the TxDOT portable type 2 PCTB with sign support assembly. Report FHWA/TX-11/0-6143-1. College Station (TX): Texas Transportation Institute; 2011.
[30] Bligh RP, Arrington DR, Sheikh NM, Silvestri C, Menges WL. Development of a MASH TL-3 median barrier gate. Report FHWA/TX-11/9-1002-2. College Station (TX): Texas Transportation Institute; 2011.
[31] Williams WF, Bligh RP, Menges WL. MASH test 3-11 of the TxDOT single slope bridge rail (type SSTR) on pan-formed bridge deck. Report FHWA/TX-11/9-1002-3. College Station (TX): Texas Transportation Institute; 2011.
[32] Bligh RP, Abu-Odeh AY, Menges WL. MASH test 3-10 on 31-inch W-beam guardrail with standard offset blocks. Report FHWA/TX-11/9-1002-4. College Station (TX): Texas Transportation Institute; 2011.
[33] Arrington DR, Bligh RP, Menges WL. MASH test 3-37 of the TxDOT 31-inch W-beam downstream anchor terminal. Report FHWA/TX-12/9-1002-6. College Station (TX): Texas Transportation Institute; 2011.
[34] Sheikh NM, Bligh RP, Menges WL. Determination of minimum height and lateral design load for MASH test level 4 bridge rails. Report FHWA/TX-12/9-1002-5. College Station (TX): Texas Transportation Institute; 2011.
[35] Sennah K, Juette B, Weber A, Witt C. Vehicle crash testing on a GFRP-reinforced PL-3 concrete bridge barrier. In: The 2011 conference & exhibition of the transportation association of Canada, Edmonton, Canada, September 11–14; 2011.
[36] Sennah K, Khederzadeh HR. Development of cost-effective PL-3 concrete bridge barrier reinforced with sand-coated glass fiber reinforced polymer (GFRP) bars: vehicle crash test. Can J Civ Eng 2012;41(4):357–67.
[37] Hampton CE, Gabler HC. Development of a missing post repair guideline for longitudinal barrier crash safety. J Transp Eng 2013;139(6):549–55.
[38] Atahan AO, Yücel AÖ, Erdem MM. Crash testing and evaluation of a new generation L1 containment level guardrail. Eng Fail Anal 2014;38:25–37.
[39] LSTC. LS-DYNA keyword user's manual, version 971. Livermore (CA): Livermore Software Technology Corporation; 2007.
[40] Ray MH. Repeatability of full-scale crash tests and criteria for validating simulation results. Transp Res Rec 1996;1528:155–60.
[41] Ray MH. Use of finite element analysis in roadside hardware design. Transp Res Circ 1996;453:61–71.
[42] Ray MH, Patzner GS. Finite element model of modified eccentric loader terminal (MELT). Transp Res Rec 1997;1599:11–21.
[43] Plaxico CA, Patzner GS, Ray MH. Finite element modeling of guardrail timber posts and the post-soil interaction. Transp Res Rec 1998;1647:139–46.
[44] Reid JD. Towards the understanding of material property influence on automotive crash structures. Thin-Wall Struct 1996;24:285–313.
[45] Reid JD. Admissible modeling errors or modeling simplifications. Finite Elem Anal Des 1998;29:49–63.
[46] Reid JD, Bielenberg BW. Using LS-DYNA simulation to solve a design problem: bullnose guardrail example. Transp Res Rec 1999;1690:95–102.
[47] Zaouk AK, Marzougui D, Bedewi NE. Development of a detailed vehicle finite element model, part I: methodology. Int J Crashworthiness 2000;5(1):25–36.
[48] Zaouk AK, Marzougui D, Kan CD. Development of a detailed vehicle finite element model, part II: material characterization and component testing. Int J Crashworthiness 2000;5(1):37–50.
[49] Zaouk AK, Bedewi NE, Kan CD, Marzouigui D. Development and evaluation of a C-1500 pickup truck model for roadside hardware impact simulation. Report FHWA-RD-96-212. Washington (DC): Federal Highway Administration; 1997.
[50] Reid JD, Marzougui D. Improved truck model for roadside safety simulations: part I – structural modeling. Transp Res Rec 2002;1797:53–62.
[51] Tiso P, Plaxico C, Ray M. Improved truck model for roadside safety simulations: part II – suspension modeling. Transp Res Rec 2002;1797:63–71.
[52] Marzougui D, Zink M, Zaouk AK, Kan CD, Bedewi NE. Development and validation of a vehicle suspension finite element model for use in crash simulations. Int J Crashworthiness 2004;9(6):565–76.
[53] Mohan P, Marzougui D, Kan C-D. Validation of a single unit truck model for roadside hardware impact. Int J Veh Syst Model Test 2007;2(1):1–15.
[54] Mohan P, Marzougui D, Meczkowski L, Bedewi N. Finite element modeling and validation of a 3-strand cable guardrail system. Int J Crashworthiness 2005;10:267–73.
[55] Plaxico CA, Kennedy JC, Miele CR. Development of an NCHRP report 350 TL-3 New Jersey shape 50-inch portable concrete barrier. Final report. Ohio Department of Transportation; 2006.
[56] Plaxico CA, Hackett RM, Uddin W. Simulation of a vehicle impacting a modified thrie-beam guardrail. Transp Res Rec 1997;1599:1–10.
[57] Marzougui D, Bahouth G, Eskandarian A, Meczkowski L, Taylor H. Evaluation of portable concrete barriers using finite element simulation. Transp Res Rec 2000;1720:1–6.

[58] Kan CD, Marzougui D, Bahouth GT, Bedewi NE. Crashworthiness evaluation using integrated vehicle and occupant finite element models. Int J Crashworthiness 2001;6:387–98.
[59] Plaxico CA, Mozzarelli F, Ray MH. Tests and simulation of a w-beam rail-to-post connection. Int J Crashworthiness 2003;8(6):543–51.
[60] Mackerle J. Finite element crash simulations and impact-induced injuries: an addendum. A bibliography (1998–2002). Shock Vibrat Digest 2003;35(4):273–80.
[61] Atahan AO. Finite element simulation of a strong-post W-beam guardrail system. Simulation 2002;78(10):587–99.
[62] Atahan AO. Impact behaviour of G2 steel weak-post W-beam guardrail on nonlevel terrain. Int J Heavy Veh Syst 2003;10(3):209–23.
[63] Atahan AO, Cansiz OF. Crashworthiness analysis of a bridge rail-to-guardrail transition. Finite Elem Anal Des 2005;41:371–96.
[64] Cansiz OF, Atahan AO. Crash test simulation of a modified thrie-beam high containment level guardrail under NCHRP report 350 TL 4-12 conditions. Int J Heavy Veh Syst 2006;13:2–18.
[65] Bligh RP, Abu-Odeh AY, Hamilton ME, Seckinger NR. Evaluation of roadside safety devices using finite element analysis. Report FHWA/TX-04/0-1816-1. College Station (TX): Texas Transportation Institute; 2004.
[66] Orengo F, Ray MH, Plaxico CA. Modeling tire blow-out in roadside hardware simulations using LS-DYNA. In: IMECE2003-55057, the 2003 ASME international mechanical engineering congress & exposition, Washington (DC); 2003.
[67] Ray MH, Oldani E, Plaxico CA. Design and analysis of an aluminum F-shape bridge railing. Int J Crashworthiness 2004;9(4):349–63.
[68] Reid JD. LS-DYNA simulation influence on roadside hardware. Transp Res Rec 2004;1890:34–41.
[69] Reid JD, Coon BA, Lewis BA, Sutherland SH, Murray YD. Evaluation of LS-DYNA soil material model 147″ FHWA-HRT-04-094. McLean (VA): U.S. Department of Transportation, Federal Highway Administration; 2004.
[70] Reid JD, Hiser NR. Friction modelling between solid elements. Int J Crashworthiness 2004;9(1):65–72.
[71] Reid JD, Hiser NR. Detailed modeling of bolted joints with slippage. Finite Elem Anal Des 2005;41:547–62.
[72] Reid JD, Kuipers BD, Sicking DL, Faller RK. Impact performance of W-beam guardrail installed at various flare rates. Int J Impact Eng 2009;36:476–85.
[73] Borovinsek M, Vesenjak M, Ulbin M, Ren Z. Simulation of crash tests for high containment levels of road safety barriers. Eng Fail Anal 2007;14:1711–8.
[74] Whitworth HA, Bendidi R, Marzougui D, Reiss R. Finite element modeling of the crash performance of roadside barriers. Int J Crashworthiness 2004;9(1):35–43.
[75] Marzougui D, Mohan P, Kan CD, Opiela KS. Evaluation of rail height effects on the safety performance of W-beam barriers. In: 2007 TRB annual meeting, Washington (DC); 2007.
[76] Mohan P, Marzougui D, Kan CD. Validation of a single unit truck model for roadside hardware impact. Int J Veh Syst Model Test 2007;2(1):1–15.
[77] Marzougui D, Mahadevaiah U, Kan CD, Opiela K. Analyzing the effects of cable barriers behind curbs using computer simulation. NCAC 2009-W-008. Washington (DC): The National Crash Analysis Center, George Washington University; 2009.
[78] Marzougui D, Mohan P, Kan CD, Opiela KS. Assessing options for improving barrier crashworthiness using finite element models and crash simulations. Final report NCAC-2012-W-008. Washington (DC): National Crash Analysis Center, George Washington University; 2012.
[79] Ferdous MR, Abu-Odeh A, Bligh RP, Jones HL, Sheikh NM. Performance limit analysis for common roadside and median barriers using LS-DYNA. Int J Crashworthiness 2011;16(6):691–706.
[80] Atahan Ali Osman, Arslan Turan. Collision behaviour of double W-beam transition. Int J Heavy Veh Syst 2012;19(1):76–91.
[81] Marzougui D, Kan CD, Opiela KS. Comparison of crash test and simulation results for impact of Silverado pickup into New Jersey barrier under manual for assessing safety hardware. Transp Res Rec 2012;2309:114–26.
[82] Marzougui D, Kan CD, Opiela KS. Crash test & simulation comparisons of a pickup truck & a small car oblique impacts into a concrete barrier. In: The 13th international LS-DYNA users conference, Dearborn (MI); 2013.
[83] Wang Q, Fang H, Li N, Weggel DC, Wen G. An efficient FE model of slender members for crash analysis of cable barriers. Eng Struct 2013;52:240–56.
[84] Fang H, Wang Q, Weggel DC. Crash analysis and evaluation of cable median barriers on sloped medians using an efficient finite element mode. Adv Eng Softw 2015;82:1–13.
[85] Fang H, Rais-Rohani M, Liu Z, Horstemeyer MF. A comparative study of metamodeling methods for multi-objective crashworthiness optimization. Comput Struct 2005;83:2121–36.
[86] Xiang Y, Wang Q, Fan Z, Fang H. Optimal crashworthiness design of a spot-welded thin-walled hat section. Finite Elem Anal Des 2006;42(10):846–55.
[87] Hou S, Li Q, Long S, Yang X, Li W. Design optimization of regular hexagonal thin-walled columns with crashworthiness criteria. Finite Elem Anal Des 2007;43:555–65.
[88] Hou S, Li Q, Long S, Yang X, Li W. Multiobjective optimization of multi-cell sections for the crashworthiness design. Int J Impact Eng 2008;35(11):1355–67.
[89] Liao X, Li Q, Yang X, Zhang W, Li W. Multiobjective optimization for crash safety design of vehicles using stepwise regression model. Struct Multidiscip Optim 2008;35(6):561–9.
[90] Horstemeyer MF, Ren X, Fang H, Acar E, Wang PT. A comparative study of design optimization methodologies for side-impact crashworthiness using injury-based versus energy-based criterion. Int J Crashworthiness 2009;14(2):125–38.
[91] Hou S, Li Q, Long S, Yang X, Li W. Crashworthiness design for foam filled thin-walled structures. Mater Des 2009;30(6):2024–32.
[92] Bi J, Fang H, Wang Q, Ren X. Modeling and optimization of foam-filled thin-walled columns for crashworthiness designs. Finite Elem Anal Des 2010;46(9):698–709.
[93] Yin H, Wen G, Hou S, Chen K. Crushing analysis and multiobjective crashworthiness optimization of honeycomb-filled single and bitubular polygonal tubes. Mater Des 2011;32:4449–60.
[94] Hou SJ, Liu TY, Dong D, Han X. Factor screening and multivariable crashworthiness optimization for vehicle side impact by factorial design. Struct Multidiscip Optim 2014;49:147–67.
[95] Jin R, Chen W, Simpson TW. Comparative studies of metamodeling techniques under multiple modeling criteria. Struct Multidiscip Optim 2001;23(1):1–13.
[96] Hou S, Zheng Y, Xie J, Han X X. Optimization design of NJ shaped guardrail based on collision safety consideration. Int J Comput Methods 2014;11:1350083-1–1350083-20.
[97] Hou S, Tan W, Zheng Y, Han X, Li Q. Optimization design of corrugated beam guardrail based on RBF-MQ surrogate model and collision safety consideration. Adv Eng Softw 2014;78:28–40.
[98] NCAC. Development & validation of a finite element model for the 1996 Dodge Neon passenger sedan. Report NCAC 2007-T-007. Washington (DC): National Crash Analysis Center, The George Washington University; 2008.
[99] NCAC. Development & initial validation of a 2007 Chevrolet Silverado finite element model. Report NCAC 2009-T-005. Washington (DC): National Crash Analysis Center, The George Washington University; 2009.
[100] NCAC. Modeling, testing & validation of the 2007 Chevrolet Silverado finite element model. Report NCAC 2009-W-005. Washington (DC): National Crash Analysis Center, The George Washington University; 2009.
[101] NCAC. Component and full-scale tests of the 2007 Chevrolet Silverado suspension system. Report NCAC 2009-R-004. Washington (DC): National Crash Analysis Center, The George Washington University; 2009.
[102] NCAC. Extended validation of the finite element model for the 2007 Chevrolet Silverado pick-up truck. Report NCAC 2012-W-003. Washington (DC): National Crash Analysis Center, The George Washington University; 2012.
[103] Hardy RL. Multiquadric equations of topography and other irregular surfaces. J Geophys Res 1971;76(8):1905–15.
[104] Box GEP, Hunter JS, Hunter WG. Statistics for experimenters: design, innovation, and discovery. 2nd ed. Wiley-Interscience; 2005.
[105] Myers RH, Montgomery DC, Anderson-Cook CM. Response surface methodology: process and product optimization using designed experiments. 3rd ed. Wiley; 2009.
[106] Taguchi G. Introduction to quality engineering: designing quality into products and processes. Quality Resources 2009.